MAGNETIC FORCE MICROSCOPY STUDY OF NEW NANOCRYSTALLINE SOFT MAGNETIC RIBBONS. M. E. Hawley , G. W. Brown, and D. J. Thoma, Los Alamos National Laboratory, Los Alamos, NM; M. A. Willard, D. E. Laughlin, and M. E. McHenry, Carnegie Mellon University, Department of Materials Science and Engineering, Pittsburgh, PA.

ABSTRACT

New nanocrystalline, multicomponent extremely soft magnetic materials with superior high temperature magnetic properties hold great promise in power applications. Fabricated in ribbon form by rapid solidification methods, the initial material is amorphous. By controlled annealing procedures, the amorphous material was transformed into a nanocrystalline form with the degree of crystallinity determined by the annealing temperature and time. The magnetic structures of ribbons, as-fabricated and annealed at temperatures from 550 to 750 °C were examined by magnetic force microscopy to determine the impact of residual stress and nanocrystallinity on the observed structure. A correlation was seen between the magnetic structures and surface microstructure. The wheel side of the as-processed ribbon was rougher than the top side of the ribbon and a complicated magnetic domain structure was present in the amorphous material. After annealing, nanocrystals formed, increasing in size with increasing temperature. The lowest temperature annealed sample had a bimodal grain size distribution and a combination of stripe and localized domains. After annealing little difference was seen between the two sides of the ribbons. Stripe domains were absent in the ribbons annealed at the highest temperatures.

INTRODUCTION

Both intrinsic and extrinsic effects play an important role in determining the ultimate properties of materials. While considerable work has focussed on chemically tuning properties, increasing attention is being directed toward understanding the role of process-induced effects such as stress and microstructure, i.e. the structure-property relationships. Although these process-induced effects can impact adversely on the functionality of the material, they can also be viewed as new degrees of freedom for producing unique tunable properties. Of particular interest here, is how they impact on the properties of magnetic alloy materials, e.g. stress-induced anisotropies in amorphous alloys [1]. In this work, a new alloy, HITPERM [2], with a composition of $(Fe_{0.5}Co_{0.5})_{88}Zr_7B_4Cu_1$, was produced in the form of amorphous melt-spun ribbons. Some ribbons were annealed at temperatures between 550 °C and 750 °C to produce nanocrystalline material. X-ray diffraction results combined with differential thermal analysis determined that the as-produced material was amorphous and that α'– FeCo crystallites form above 510 °C with secondary crystallization of small amounts of $(FeCo)_3Zr$ appearing above 700 °C. The addition of Zr and B is believed to aid glass forming properties while a small amount of Cu depresses the temperature at which α'– FeCo crystallites form.

Previously, atomic and magnetic force microscopies (AFM and MFM) were used to study amorphous $Fe_{80}B_{16}Si_4$ alloy ribbons [3]. In that study, stress was deliberately introduced in the ribbon by bending and the subsequent stress-induced microstructures and magnetic structures were studied. In that case, the MFM data faithfully reproduced the results obtained by more traditional techniques [4]. Although MFM, at this time, cannot give unambiguous quantitative

Mat. Res. Soc. Symp. Proc. Vol. 577 © 1999 Materials Research Society

magnetic information, that study demonstrated that it is powerful tool for revealing detailed relatively high resolution (10's of nanometers) magnetic structure information.

In the present study, AFM and MFM were used to study the micro- and magnetic structure of HITPERM ribbons resulting from the fabrication and annealing processes. This alloy is particularly attractive for use in high temperature applications because it retains a high magnetization to elevated temperatures (> 900 °C). The as-produced HITPERM ribbons produced in the melt-spinning process are amorphous. HITPERM has a non-zero magnetostrictive constant and is, therefore, subject to a number of factors during the fabrication and annealing processes that can lead to the formation of magnetic domains. Magnetoelastic effects during production due to a temperature gradient between the top and bottom sides of the ribbons as it is melt-spun, can result in residual stress creating a magnetic easy axis along a tensor direction. Annealing is often used to relieve this stress and eliminate magnetic domains and resulting ac losses. In this case, the annealing temperatures were deliberately chosen to create a nanocrystalline material to tailor magnetic properties by creating a two phase system composed of two magnetic phases, a nanocrystalline phase and an amorphous grain boundary phase. The current work is part of an ongoing study.

EXPERIMENTAL

Ingots of $Fe_{44}Co_{44}Zr_7B_4Cu_1$ were fabricated by arc melting electrolytic Fe(99.9% pure – low carbon), Co (99.9% pure), Fe_3B (90.75% metals basis), and Cu (99.9% pure) in an argon atmosphere. Amorphous ribbons were produced from the ingots using a single wheel melt spinning technique [5]. The melt spinning process involved remelting the arc-melted ingot in a boron nitride crucible in an argon atmosphere. A small positive pressure of argon was then used to quench the molten alloy onto the Cu-Be wheel rotating at 35 m/s. The ribbons produced by this procedure were approximately 1 mm wide and 20 to 50 μm thick. Following the melt spinning procedure, sections of the ribbon were isothermally annealed for 1 hour at 550 °C, 650 °C, or 750 °C in an inert (argon) atmosphere followed by a water quench. The annealing and quenching procedure produced nanocrystalline microstructures.

The ribbons were characterized using AFM and MFM. The microstructure, obtained in TappingMode™, and the force gradient magnetic structure, taken in constant-height lift mode, were acquired in a two-pass method that yields a one-to-one correspondence between microstructure and magnetic domain structure. Three types of commercially available magnetically coated Si tips were used for imaging. High coercivity (HC), moderately high coercivity CoCr, and superparamagnetic Fe/SiO_2 coated tips were used. Prior to imaging, the tips were polarized normal to the sample surface. To minimize the effect of static charges on the magnetic imaging, data was collected in an isolation box with moisture introduced by a humidifier (~45% relative humidity). The samples were grounded to the probe ground via a Cu strip.

Field-dependent MFM data were collected on the 550 °C ribbon. Preliminary field-dependent data were also collected on the 650 °C ribbon but will not be presented here. An external

permanent magnet was used to apply an in-plane field of 34 to 250 Oe with MFM scans taken at a 25 to 50 Oe increment.

Very preliminary potentiometric measurements were made on some of the ribbons using the conductive magnetic tips. Typically 2 volts DC were supplied by a battery with a 22 MΩ current limiting resistor in series with the sample. 2 V AC was applied to the tip.

RESULTS

Figure 1 is a composite 15 μm x 15 μm images of the microstructures of the ribbons with their corresponding magnetic domain structures. The as-produced HITPERM ribbon appeared to be amorphous, i.e. no nanocrystalline structure was observed by AFM (Figure1a). The corresponding magnetic structure for this ribbon (Figure 1a - column 2) consisted of inclusion surrounded by a complicated array of parallel domain walls. Many of those walls appear to emanate from the inclusions. At the annealing temperatures selected in this study, nanocrystals were formed, at least on the surface of the treated ribbons, increasing in size with increasing temperature. As can be seen in Figure 1b, the ribbon annealed at 550 °C had a bimodal distribution of nanocrystal sizes (about 200 to 300 nm and 350 to 500 nm). Its magnetic structure (Figure 1b - column 2) consisted of stripe domains where the smaller crystallites existed and localized domains located in the larger crystallite regions. By 650 °C (Figure 1c), the surface RMS roughness of the ribbon had increased from about 40 nm for the 550 °C ribbon to around 60 nm. This increased roughness was a reflection of the wide distribution in crystallites sizes, ranging from 100 nm to over 700 nm for minority crystallites. The magnetic structure of the 650 °C ribbon (Figure 1b - column 2) consisted of a combination of meandering stripe walls/domains containing localized single domains located at the position of larger crystallites. The 750 °C ribbon surface crystallites were larger and more uniform in size, clustered between 450 nm and 650 nm with a surface RMS roughness of over 80 nm. The crystallites also appear more faceted, some showing the beginnings of island growth. The increased faceting suggests that these nanocrystals have improved crystal quality. One has to emphasize that all of the images are of the ribbon outer surface and do not necessarily reflect the structure of the interior.

A comparison between the differences in the microstructure and magnetic structure for the two sides of the as-processed ribbon and the ribbons annealed at 550 °C and 650 °C is presented in Figure 2a and 2b and Figure 2c and 2d, respectively. Although the wheel sides of these ribbons were rougher than their corresponding upper surface, the most dramatic difference existed for the as-prepared ribbon, Figure 2a and 2b column 1. The structure of the wheel side of the amorphous ribbon probably reflected the roughness of the surface of the wheel itself. The bottom sides of the ribbons annealed at 550 °C and 650 °C were only slightly rougher than their corresponding top sides (Figure 2a and b – column 2 and 3). The differences were not significant and might only reflect the particular selected area imaged. The annealing process led to the formation of nanocrystals on both sides of the ribbons, reducing the initial fabrication differences. The differences in structure between the upper side of the ribbons and their respective wheel side were also reflected in the magnetic structures, Figure 2c and 2d, and were again most notable for the as-fabricated ribbon. As mention above, the magnetic structure for the top side of that ribbon appears to consist of stress lines radiating out from inclusions. The character of the magnetic structure on the wheel side (Figure 2d – column1), although it had features running in the same

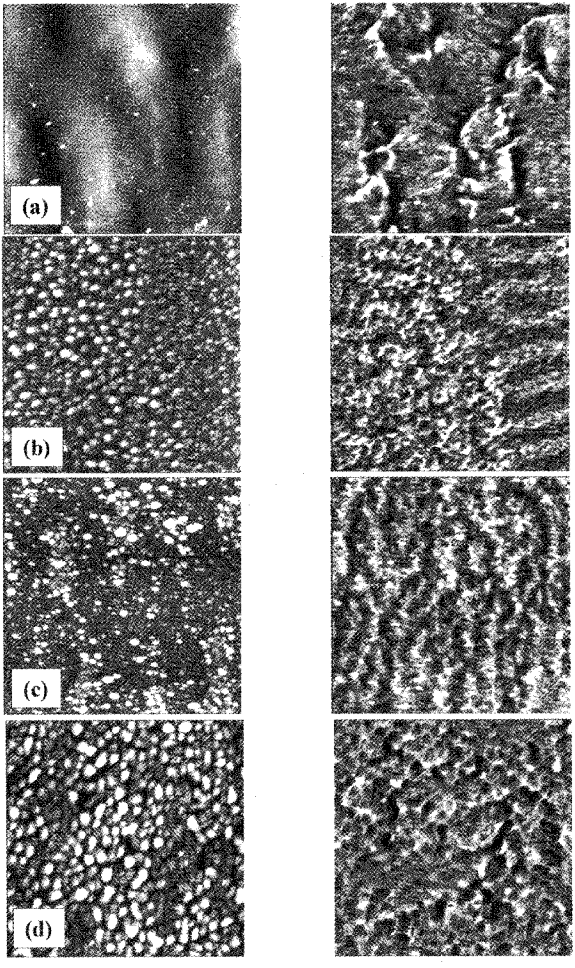

Figure 1. AFM (first column) and MFM (second column) 15 μm x15 μm images of the surfaces of $Fe_{44}Co_{44}Zr_7B_4Cu_1$ alloy ribbons: a) as-processed, b) 550 °C anneal, c) 650 °C anneal, and d) 750 °C anneal.

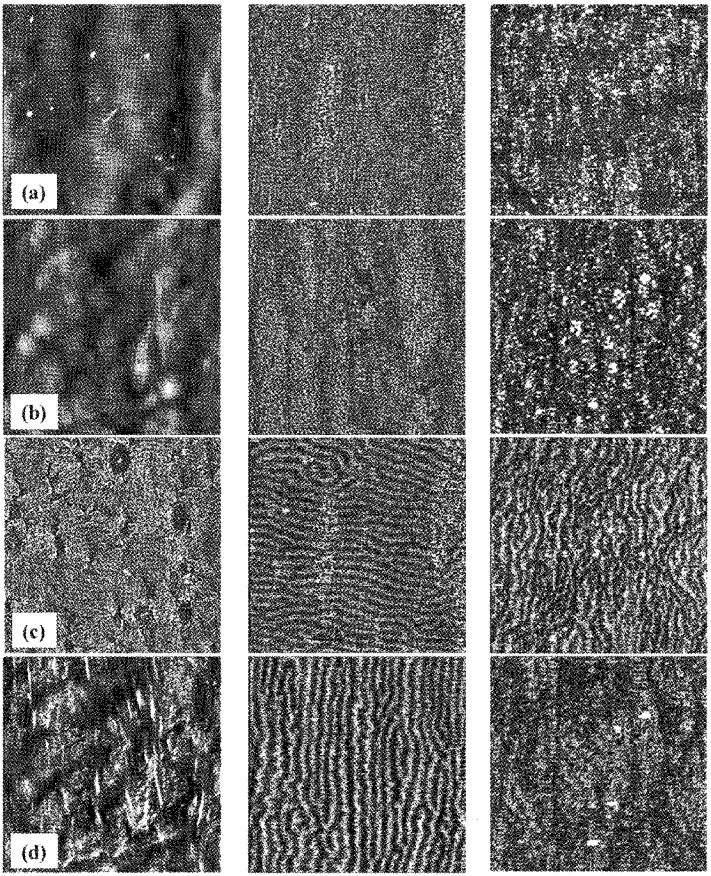

Figure 2. AFM, rows (a) and (b), and MFM, rows (c) and (d), 40 μm x 40 μm images of the surfaces of $Fe_{44}Co_{44}Zr_7B_4Cu_1$ alloy ribbons: Rows (a) and (c) are the top side of the ribbon, rows (b) and (d) are the wheel side. First column is the as-fabricated ribbon, the middle column was annealed at 550 °C, and the last column is the sample annealed at 650 ° C.

direction as the ribbon length, was too complicated to allow analysis. As noted above, the magnetic structure for the 550 °C ribbon - top and bottom (Figure 2c and d – column 2), and 650 °C ribbon - top (2c – column 3) had stripe or meandering stripe domains. Only the 550 °C ribbon had similar magnetic structures on both surfaces. The 650 °C ribbon – bottom appeared to have only localized domains. Again, these observations were limited to the small areas characterized. No extended domains were observed for the 750 °C ribbon. The magnetic structure for this ribbon, Figure 1, appeared to be localized to the individual crystallites. The correlation between the magnetic structure and microstructure is apparent from these images. The differences in the magnetic structures shown in Figure 1 reflect the evolution of the microstructure as the annealing temperature was increased and the average nanocrystallite sizes increased. The differences in Figure 2 reflect the thermal stress across the ribbons during fabrication and cool down and how the annealing temperature affects these differences.

Table I. Summary of crystallite sizes and surface RMS roughness.

Sample	Crystallite Size (nm)	RMS Roughness (nm)
Amorphous Top	N/A	7.7
Amorphous Wheel Side	*3 μm – 8 μm structural features	77
550 °C Top	200 – 300 & 350 - 500	40
550 °C Wheel Side	230 - 400	51
650 °C Top	150 - 350	50
650 °C Wheel Side	100 - 700	60
750 °C	450 - 650	80

Table I summarizes the microstructural data from Figure 1 and Figure 2. The spread in crystal size is shown in Table 1, not the average size.

Figure 3 is another topographic/magnetic 15 μm x 15 μm image set of the top surface of the as-processed ribbon, this time taken with a HC magnetic tip. These images clearly show a vortex-like the relationship between the inclusion and the surrounding magnetic structure. The magnetic image is free of streaks, a clue to the magnetic hardness of this stress-induces domain structure.

One concern with MFM imaging is the influence of the tip on the sample's magnetic structure and, therefore, the resulting MFM image. One counter strategy is to use tips with different magnetic hardness, in particular a very hard tip whose magnetic structure that isn't altered by the sample and a very soft tip whose magnetization is changes spontaneously under the influence of domains in the sample's. Figure 4 contains images taken with a paramagnetic tip of the amorphous (a) and 550 °C (b) and 650 °C (c) annealed ribbons. A comparison with the corresponding images in Figure 2 reveals very little differences, giving confidence that the field from the MFM tip has had little effect on domain structures of these ribbons.

In an attempt to identify whether the annealed ribbons had nonconductive phases, preliminary surface potential imaging was attempted. This technique could potentially eliminate some of the uncertainty in interpretation of some features in the magnetic images, i.e. whether structures in the MFM images are due to the presence of nonmagnetic material or whether they are due to the presence of in-plane magnetic domains. Briefly, this scanning probe two-pass technique using a conductive tip, the first pass in standard tapping mode to obtain the topography and the second pass in a nonvibrating mode but with oscillating voltage, $V_{ac}Cos\ \omega t$, applied to the tip and a DC voltage applied across the sample. This results in an oscillating electrostatic force $F = dC/dz V_{dc} V_{ac}$ on the cantilever at the ac frequency ω where dC/dz is the tip-sample capacitance gradient and V_{dc} is the voltage difference between the tip and the sample. The technique entails sensing variations in the voltage difference resulting from local variation in resistance within the sample. An equal and opposite voltage is applied to the tip to create a null voltage difference. Since the oscillating electrostatic force, F, is the product of the ac and dc components and $V_{dc} = 0$, the electrostatic force is also zero. The value of the applied field to the tip needed to accomplish the null condition becomes the intensity scale on the potentiometric image. Like the MFM technique, the technique is sensitive to changes within the sample not just the surface. Figure 5 is an image taken by this technique and reveals some areas over the 40 μm x 40 μm region where the resistivity is higher (brighter in the image). Although the impetus for using this technique was to identify nonconductive material in the ribbons, it is not possible at this time to speculate as to the actual origin of this variation in resistance and the resolution in this image is too low to identify individual insulating inclusions.

Finally, although field-dependent magnetic hysteretic data has not collected for any of these ribbon, MFM data was collected for the 550 °C ribbon at different values of in-plane external field applied via a permanent magnet. Data was collected for field values from 34 Oe to over 250 Oe. A selection of the images taken within this field range is presented in Figure 6 to show the evolution of the domain structure. By 34 Oe, the lowest field possible in the present experimental setup, the local domains had disappeared, leaving behind only the maze-like structure. As the field was increased to 100 Oe the spacing between domains decreased from about 2.4 μm to around 1.6 μm with a concomitant decrease in the number of branches resulting in a more stripe-like structure. The domain spacing was further reduced to about 1.3 μm at 125 Oe, 1.1 μm at 150 Oe, 0.9 μm at 200 Oe, and unmeasureable at 250 Oe. The wider stripes at the bottom of Figure 6f are probably due to electrostatic effects. The decrease in intensity of the MFM signal is primarily due to the rotation of the magnetization into the plane of the sample. The light and dark contrast in these images depend on whether the stray field out of the sample is aligned anti- or parallel to the tip magnetization direction. The only information about in-plane magnetic structure is indirect, that is the domain spacing observed at various fields between light and dark regions is

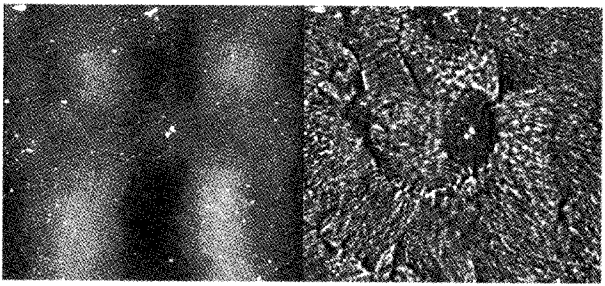

Figure 3. AFM and MFM 15 μm x 15 μm images taken on as-fabricated ribbon. The magnetic image (right) revealed an apparent inclusion not obvious in the topograph (left).

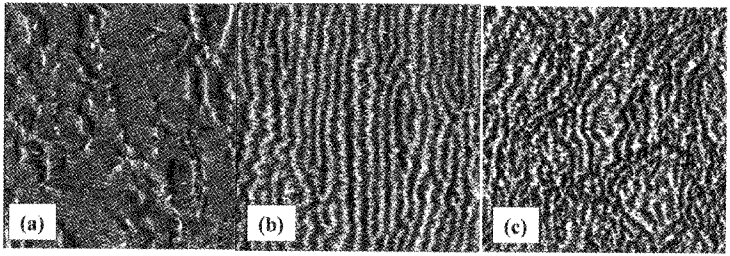

Figure 4. MFM 40 μm x 40 μm images taken on $Fe_{44}Co_{44}Zr_7B_4Cu_1$ alloy ribbons (a) as-fabricated, (b) annealed at 550 °C, and (c) annealed at 650 °C. These images were taken with superparamagnetic Fe/SiO_2 coated tips.

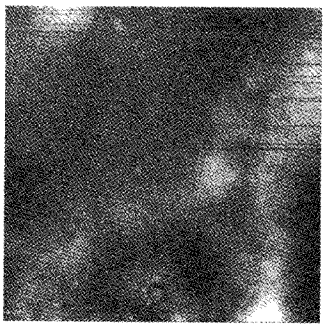

Figure 5. Preliminary 40 μm x 40 μm potentiometric image taken on a $Fe_{44}Co_{44}Zr_7B_4Cu_1$ alloy ribbons annealed at 550 °C with CoCr coated tips.

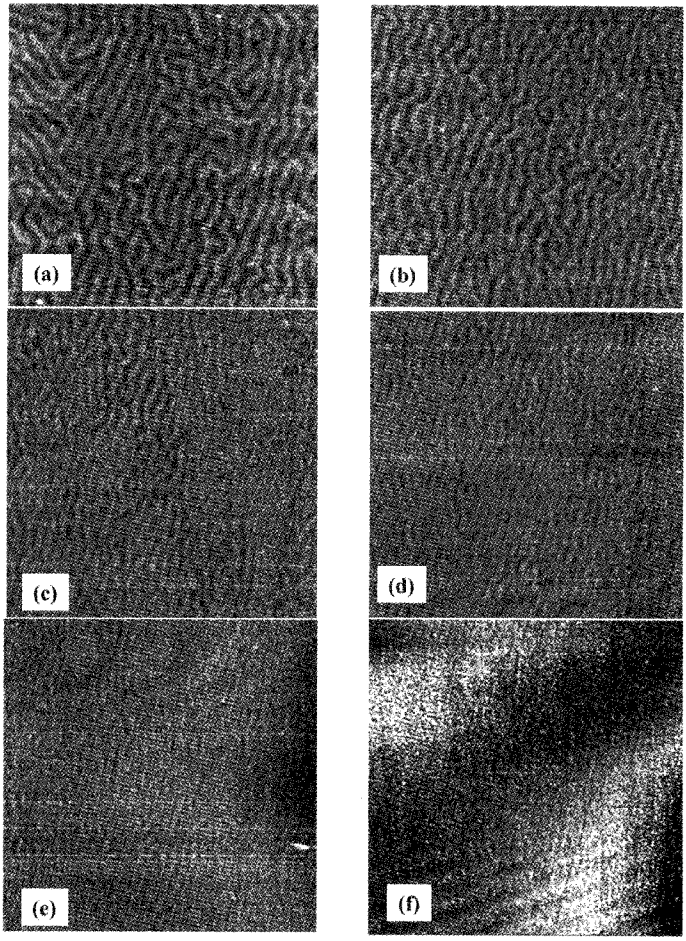

Figure 6. MFM 40 μm x 40 μm images taken on an alloy ribbon annealed at 550 °C with an in-plane magnetic field of (a) 34Oe, (b) 100Oe, (c) 125Oe, (d) 150Oe, (e) 200Oe, and (f) 250Oe.

uniform suggesting that any in-plane magnetization is oriented in approximately the same direction across the sample. Although not presented here, preliminary field-dependent MFM measurements on the 650 °C ribbon show the same trend. Note that this investigation examined the evolution of the domain structure for a field applied parallel to the ribbon thickness. Geometric (demagnetization) effects will cause the fields required to be much larger than if the field were applied along the ribbon length as would be the case in a toroidal core, for example.

DISCUSSION

The AFM data on the HITPERM ribbons revealed the evolution in the microstructure from the amorphous as-produced form to a nanocrystalline structure above 550 °C due with both crystal size and faceting increasing with increasing temperature. The low crystallization temperature is principally due to the addition of Cu. MFM measurements of the out-of-plane sample stray field reflect these microstructural changes evolving from magnetoelastically driven domains radiating from inclusions to maze or stripe domains due to both local exchange and longer range interactions. The magnetic structure of the larger nanocrystalline, higher temperature annealed ribbons appear monodomain and localized. One difficulty, however, remains in interpreting the MFM data, i.e. distinguishing between nonmagnetic areas from in-plane magnetization. This is particularly true when a large amount of complicated structure is present in the images. The complicated structures seen for the amorphous ribbon and those ribbons annealed at the higher temperature where phase separation is likely. In addition, some features in the magnetic images could be due to electrostatic effects or damping of the cantilever oscillation from other tip-sample interactions. The situation is complicated in the case of the field-dependent measurements when the in-plane applied fields approach the coercivity of the tip magnetic coating. The magnetization orientation of the tip in this case is expected to start rotating in response to the field in a direction cant to the sample surface normal as the external in-plane field approaches the coating coercivity. Nonetheless, the MFM measurements reveal some interesting trends in the evolution of the microstructure and corresponding magnetic structure as the as-fabricated sample was annealed at increasing temperatures.

The field-dependent MFM data does not reflect directly what is happening with the in-plane magnetization. As mentioned above it can give indirect information about whether in-plane domains are aligned anti parallel or not. It doesn't tell you how much of the magnetization is out-of-plane versus in-plane. The MFM data is not a substitute for vibrating sample magnetometry data but compliments that information. For instance, the MFM may shed light on why a hysteretic loop is not square due to out-of-plane magnetization due. The MFM-field data can also tell you about wall pinning and wall motion. The MFM is a powerful tool for revealing the presence and nature of domain structures as well as the presence of magnetoelastic effects to aid in interpretation of bulk type measurements.

SUMMARY

The magnetic images of the amorphous ribbon show that the magnetic structure is probably due to magnetoelastic effects from residual stresses present upon cooling. Inclusions, are more visible in the magnetic images, forming a vortex for magnetic domains. The complicated

magnetic domain structure for the annealed samples reflects the presence of the nanocrystals. Stripe domains were present in the 550 °C ribbon and persisted somewhat in the 650 °C sample but were absent in the ribbon annealed at the highest temperatures. As the nanocrystals became larger the domains became more localized. The sample annealed at the highest temperature had localized domains, each nanocrystal having a single domain..

REFERENCES

1. S. Chikazumi, Physics of Ferromagnetism, 2nd Edn., (Oxford University Press, N.Y. 1997), p. 339.
2. M. A. Willard, D.E. Laughlin, and M.E. McHenry, *J. Appl. Phys.* **84 (12)**, 6773 (1998).
3. M.E. Hawley, G.W. Brown, D.J. Markiewicz, F. Spaepen, E.P. Barth, *J. Magn. & Magn. Mat.* **190**, 89 (1998).
4. V. Lakshmanan, J.C.M. Li, *Mat. Sci. Eng.* **98**, 483 (1988).
5. D. J. Thoma, E.M. Schwartz, S.R. Bingert, D.R. Korzekwa, R.D. Field, and L.A. Jacobson, "Microsegregation during Melt-Spinning of Dilute Palladium Alloys" in Melt Spinning, Strip Casting and Slab Casting, eds. E.F. Matthys and W.G. Truckner (TMS, Warrendale, PA) p. 173-184 (1995).